J Solid State Electrochem (2008) 12:303–313
DOI 10.1007/s10008-007-0392-3

ORIGINAL PAPER

An SFG and DFG investigation of Au(111), Au(100), Au(110) and Au(210) electrodes in contact with aqueous solutions containing KCN

Benedetto Bozzini · Bertrand Busson · Gian Pietro De Gaudenzi · Claudio Mele · Abderrahmane Tadjeddine

Received: 21 March 2007 / Revised: 20 June 2007 / Accepted: 13 July 2007 / Published online: 3 August 2007

Abstract In this paper, the behaviour of Au(111), (100), (110) and (210) electrodes in contact with pH-neutral aqueous solutions of KCN has been studied as a function of potential by means of in situ sum frequency generation (SFG) and difference frequency generation (DFG) spectroscopies. The contribution of both free and bound electrons has been included. Spectroelectrochemical results were complemented with cyclic voltammetric measurements. The main emphasis in this work has been placed on systematising and quantifying the interaction between the vibrational and electronic structures of the electrodic interfaces studied by the systematic comparison of SFG and DFG spectra measured under the same electrochemical conditions for different crystal orientations.

Keywords SFG · DFG · Cyanide · Au · Single-crystal

B. Bozzini (✉) · G. P. De Gaudenzi · C. Mele
Dipartimento di Ingegneria dell'Innovazione, Università di Lecce,
v. Monteroni,
73100 Lecce, Italy
e-mail: benedetto.bozzini@unile.it

B. Busson
CLIO-LCP, Université Paris-Sud,
91405 Orsay Cedex, France

A. Tadjeddine
UDIL-CNRS, Bat. 201, Centre Universitaire Paris-Sud,
BP 34, 91898 Orsay Cedex, France

Introduction

A considerable corpus of spectroelectrochemical data is available for CN^- adsorbed onto Au. CN^- is typically adsorbed from KCN or NaCN solutions as a function of applied potential by two approaches: (1) directly in the spectroelectrochemical cell, (2) in a separate cell; the adsorbed layer is subsequently transferred into a different electrolyte where it is studied spectroelectrochemically. Spectroelectrochemical work on CN^- adsorption onto polycrystalline Au based on surface enhanced Raman spectroscopy (SERS) [1, 2] and infrared (IR) [2–5] mainly pointed towards an understanding of static and potential-dependent behaviour of the CN^- stretching band. Potential-dependent IR and SERS spectra for the Au/CN^- system yield very similar results. The CN^- stretching band at about 2,100 cm^{-1} is attributed to linearly adsorbed CN^- and $Au(CN)_2^-$ as a function of applied potential. Insight into the nature of adsorption sites for the Au/CN^- system was also gained by combined ex situ SERS and tip-enhanced Raman spectroscopy (TERS) experiments carried out with samples emersed at controlled potential and tested in air [6]; STM tip-induced frequency shifts for the CN^- stretching vibration are observed and explained with a field distribution effect developing underneath the tip apex. Differences in the inhomogeneous broadening obtained in SERS and TERS lean support to this interpretation. Details on the CN^- adlayers formed on Au(111) were obtained by in situ STM and ex situ LEED and AES [7]. Two different structures for the AuCN adlayer were found by STM: incommensurate structures of $p(1.15\times\sqrt{3}R-30°)$ and $p(1.41\times2\sqrt{3}R-30°)$ on the positive and negative sides of the voltammetric peak at ca 0.15 V vs SCE corresponding to AuCN formation. The transformation between the two

adlayer structures was shown to be reversible. Ex situ LEED and AES results confirm the structural interpretation of in situ STM data.

Recent theoretical works based on quantum chemical methods [8, 9] discuss the nature of the stretching band and Raman shift values for various adsorption configurations and chemical bonding modes. In [9], it is concluded from periodic DFT calculations that the mode observed at ca 2,100 cm^{-1} corresponds to the stretching vibration of CN adsorbed atop on (100) and (110) sites; the computed adsorption energy on (111) sites resulted to be much weaker.

In [10], the potential-dependent DFG spectra of Au (110), Au(100) and Au(111) electrode, in contact with an aqueous electrolyte consisting of $NaClO_4$ 0.1 M and KCN 0.025 M have been studied. In [11], SFG experiments were reported for Au(111) and Au(210) in the same electrolyte, but with pre-adsorption of CN^- at −600 mV vs Ag/AgCl. A comparison of DFG and SFG spectra on a Au (100) electrode in contact with an aqueous electrolyte consisting of $NaClO_4$ 0.1 M and KCN 0.05 M at a single potential (E=−800 mV vs Ag/AgCl) has been reported in [12]. The results of [10, 11] show one potential-dependent resonance, indicating the presence of one band localised within the CN^- stretching spectral range. These results reveal that some SFG observables are affected by the orientation of the single-crystal electrode, while some others are not. While the disappearance of the resonance upon oxidation of the adsorbed CN^- layer is completed at the same potential regardless of the crystal face, the potential at which the adsorption starts depends on the electrode surface orientation: CN^- adsorption starts at −1300 mV vs SCE on Au(110), −1,000 mV vs SCE on Au (100) and −800 mV vs SCE on Au(111). This observation indicates that electrode–adsorbate interactions are stronger on the more open (110) surface and decrease as the surface becomes denser [10]. These results have been confirmed also by comparing the SFG behaviour of Au(111) and (210) subjected to a pre-adsorption routine [11]. The sequence of the potentials corresponding to the inception of CN^- adsorption follows the trend in the value of the pzc for the respective faces: the most positive value is found for the (111) orientation and the most negative one for the (110) surface. The authors suggest that information regarding the mechanism and the energetics of CN^- adsorption can be gleaned from the position of the potential of adsorption onset relative to the pzc of each surface orientation in CN^--free solutions. This behaviour has been interpreted as due to a weaker adsorbate–adsorbate repulsion depending on the degree of openness of each face. The DFG resonance is markedly reduced around 0 V vs SCE for all three orientations, denoting that the kinetics and the dynamics of the CN^- desorption processes are faster on Au(111) than on Au(100) and Au (110). The rate of CN^- adsorption, as measured by the slope of the growing part of the curves, is roughly the same for all surface orientations, whereas the rate of CN^- desorption, as measured by the slope of the decreasing part of the same curve, is much higher for the (111) orientation. The DFG resonance peak frequency obeys a quadratic potential dependence, increasing from 2,090 cm^{-1} at −1,300 mV vs SCE to 2,130 cm^{-1} at 0 mV vs SCE. The potential dependence of the DFG resonance frequency (Stark effect) is the same for all the surface orientations investigated. This behaviour has been interpreted as implying that CN^- is bound tightly to the gold surface in just one—probably on top—configuration and experiences primarily the electric field of the surface atom on which it is adsorbed. The DFG results show the constancy of the full-width at half-maximum resonance with either the electrode potential or the surface orientation at the constant value of 17 cm^{-1}. This behaviour has been interpreted as due to a homogeneous broadening mechanism, coherent with the existence of a single adsorption site for CN^- on Au. The results of the comparison between SFG and DFG show that the ratio of the intensity of the non-resonant signal to the resonant one is reduced by one order of magnitude, switching from SFG to DFG, making DFG a more convenient probe of the vibrational properties of the adsorbates on Au. The CN^- adsorption range can be extended to achieve information relevant to metal-plating conditions in which CN^- is produced at the electrode surface by reduction of the Au (I)- or Au(III)-cyanocomplexes by preadsorbing CN^- [11]. The Stark-tuning was measured also at higher cathodic polarisations and confirmed the values reported in [10].

Dynamic SFG work has been reported on the Au/CN^- system. The vibrational relaxation of CN^- on polycrystalline Au in 0.1 M $NaClO_4$, KCN 0.025 M was studied by picosecond SFG in [13, 14]. Vibrational decay curves exhibit a simple exponential behaviour, which was interpreted with a strongly potential dependence T_1, ranging from 10 to 19 ps on Au; longer lifetimes were found at more positive potentials. The vibrational lifetimes and their potential dependence were described with an image-dipole theory, although the role of a charge-transfer mechanism could not be ruled out. Comparison among Ag, Au, Cu and Pt electrodes showed that the T_1 lifetimes follow a trend that is dictated by the ionic character of the metal–adsorbate bond: covalent systems, such as CN^-/Pt have shorter lifetimes than systems with more ionic character, such as CN^-/Ag, Au, Cu. In addition, a trend was noted between vibrational lifetime and the onset of interband transitions.

It has been pointed out in previous research in this group that the action of free cyanide released by the reduction of

Au(I) and Au(III) cyanocomplex on specific crystal faces can be a cause of morphological changes and mechanical instability of the electroplates. The toxic additives like Tl^{+}, Cd^{2+} and As^{3+}, which are customarily used in the Au plating industry, have been found: (1) to act on CN^{-}-related self-inhibition processes and (2) to control the hydrogen evolution reaction (HER) side, which is liable to have major impact on the electroplated and, in particular, electroformed end products. Although a good deal of very accurate work has been published about the CN^{-}/Au system, more insightful molecular-level and single-crystal work on the adsorption of CN^{-} is still needed to enhance understanding and predictive capacity in the modelling of metal plating processes and in dealing with hysteretic and irreproducibility phenomena. This is particularly critical in advanced technological fields such as the fabrication of electronic devices where the potential capabilities of electrodeposition processes need to prove to be under control and highly reproducible to forge their way into innovation in the field and compete with physical metallisation methods. This is particularly true for next-generation interconnect metallurgies where silver and gold alloys are going to play a key role in the pursuit of extreme miniaturisation where electrochemical Cu proves inadequate.

In this paper, we focus on the details of the dependence of SFG and DFG spectra on crystal orientation and potential, with the aim of elucidating the nature of the surface CN^{-} species. Both the resonant and non-resonant parts of the spectra have been analysed in an attempt to work out the synergy between CN^{-} adsorption and variations of the electronic structure of the substrate resulting from the adsorption process. The ultimate aim was to collect fundamental information, expected to have a bearing on the electrodeposition processes from cyanocomplex systems. This information can be fed into electrocrystallisation models able to predict 3D growth and morphology development. Apart from specific interest for electroplating, the present work also extends the fundamental knowledge of the Au/CN^{-} system in that it considers a complete set of crystal orientations ranging from low-index to high-index and it compares potential-dependent DFG and SFG spectroscopies.

Materials and methods

The solution employed was: KCN 25 mM, $NaClO_4$ 0.1 M. Analytic grade chemicals were dissolved in ultrapure water of conductivity 18.2 MΩ cm obtained with a Millipore Milli-Q system. Voltammetric experiments with the $NaClO_4$ 0.1 M supporting electrolyte were run for comparison. The working electrodes were single-crystal discs of Au(111), Au(100), Au(110) and Au(210) from Mateck of 3-mm diameter and 4-mm thickness cut with a precision better than 0.2°. The crystals were flame-annealed in a butane flame and quenched in ultrapure water according to the procedure recommended in [15]. Results concerning polycrystalline Au, treated the same way, are also reported for comparison; a more insightful presentation of the behaviour of polycrystalline electrodes can be found in [16].

SFG spectra were recorded in the potential range −1,200 to 0 mV vs Ag/AgCl spanned in steps of 200 mV. The electrodes were immersed in the CN^{-}-containing solution at open circuit; the potential was subsequently stepped in the negative direction and back. To check the presence of irreversible or hysteretic processes and to make sure that serial correlation among spectra is absent, a control spectrum was run at −1,200 mV at the end of the anodic-going potential staircase. In all cases, the first spectra measured at the same potential and the last one overlapped remarkably well, demonstrating the cleanliness and reproducibility of the experiment.

The SFG setup used here is analogous to the system described in [17]. Briefly, a flash-pumped YAG laser produces 15-ps pulses with a 100-MHz repetition rate. These pulses form 1-μs-long trains with a 25-Hz repetition rate. After amplification, the YAG pulses are used to pump two non-linear crystals in parallel. The first one (BBO) receives 30% of the YAG pump to produce a green 532-nm laser beam through second harmonic generation. The remaining 70% pumps an $AgGaS_2$ crystal in an optical parametric oscillator which delivers a tunable infrared wavelength between 2.7 and 6 μm. The two laser beams are then spatially and temporally overlapped at the surface of the gold electrodes to produce SFG and DFG. Both beams are p-polarized, with angles of incidence 55 and 65° for the green and infrared beams, respectively. The energy resolution of the system is 2 cm^{-1}. The electrochemical setup allows performing cyclic voltammetry and SFG/DFG experiments in the same cell. It consists of a Kel-F body, closed by a CaF_2 prism and filled with electrolyte deaerated by Ar bubbling. Inside the cell, the gold crystal is fixed to a central stub and kept in contact with a gold wire by aspiration. A three-electrode configuration is used, with a platinum wire counter electrode and an external Ag/AgCl reference (saturated KCl) electrode. For experimental purposes, the electrode is either gently pushed against the CaF_2 prism to carry out SFG/DFG measurements in a thin layer configuration or raised about 0.5 cm above the prism to perform cyclic voltammetry (CV) experiments. A scan rate of 100 mV s^{-1} has been

employed. Values reported after the symbol '±' refer to one standard deviation. Potentials are reported vs Ag/AgCl.

Results and discussion

Cyclic voltammetry

$NaClO_4$ solution

To assess the surface quality of the single crystals used in this work, CVs have been recorded in contact with the $NaClO_4$ 0.1 M supporting electrolyte solution in the potential range employed for spectroelectrochemical work in the presence of CN^- (Fig. 1). The potential range considered spans the double-layer charging region (well negative of the pzc for Au(111) and Au(100) and close to the pzc for Au(110) and Au(210) [18–21]) and the onset of the HER. The voltammetric features reported in Fig. 1 very closely match those reported in the literature for these Au (hkl) faces in cognate electrolytes.

In the high cathodic range, the HER gives rise to a faradaic current, whose intensity ranks as (110)>(100)≅(111)>(210). These results are coherent with literature results in perchlorate solutions [19, 20]. The c.d. growths visible at potentials higher than 0 mV on the negative-going scans are related to double-layer capacitance variations occurring on approaching the pzc [22] and, in the case of Au(111), (100) and (110), to surface structural variations related to reconstruction at potentials more cathodic than the pzc and incipient lifting of the reconstruction on approaching the pzc from the cathodic side [19, 22]. It is worth noticing that the Au(210) face, which does not reconstruct [18, 22, 23], displays a much less pronounced c.d. growth.

Voltammetric pzc necking can be appreciated for Au (210) at ca −100 mV (see [18]). The humps centred at ca −625 mV, well visible and corresponding to negative and positive current densities, have been proposed in [19] as a signature of surface and electrolyte cleanliness for Au(111) electrodes. A similar, although less pronounced, feature is also visible with Au(210) and Au(100) surfaces at potentials more cathodic than for Au(111); the existence of this feature seems to be related to a lower activity for the HER and might be related to structural rearrangements accompanying the proton reduction processes [24, 25].

$NaClO_4$/KCN solution

CVs for the four investigated single-crystal electrodes and for the Au polycrystal in contact with the $NaClO_4$ 0.1 M, KCN 25 mM solution are shown in Fig. 2. These data are in overall accordance with the results reported for Au(110), Au(100) and Au(111) and polycrystalline Au electrodes in the same electrolyte in [10] and references therein contained and for Au(210) [11]. The literature cathodic-going scans for single-crystal electrodes display one cathodic peak (*D*)—due to CN^- desorption—whose position depends on the crystal orientation. The literature anodic-going scans exhibit a sequence of anodic features (A, B, C) whose positions are, again, a function of the

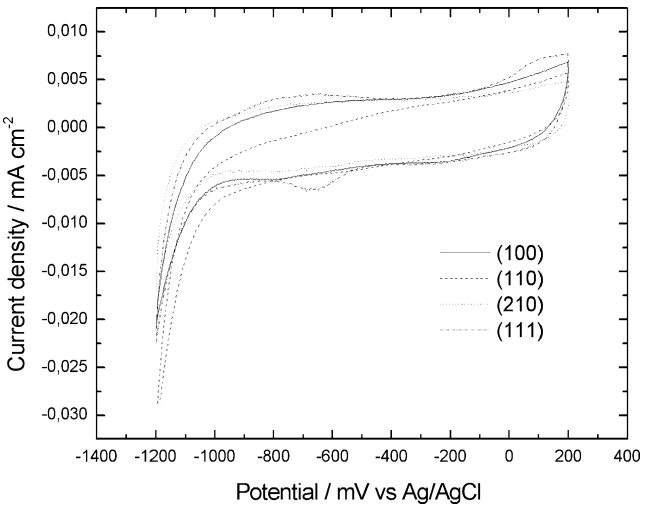

Fig. 1 Cyclic voltammetry of Au(111), (100), (110) and (210) electrodes in contact with a $NaClO_4$ 0.1 M solution ; scan rate 100 mV/s

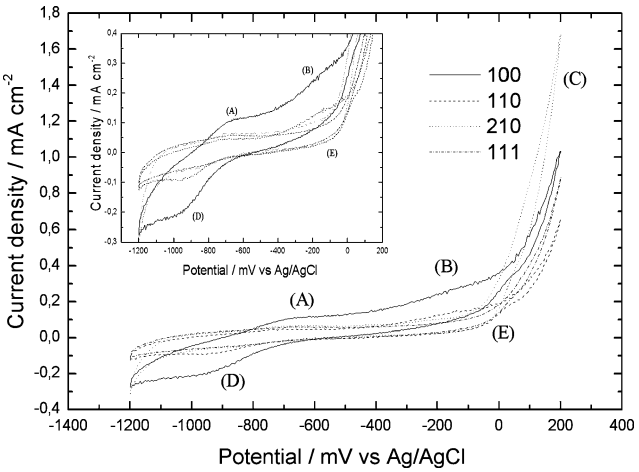

Fig. 2 Cyclic voltammetry of Au(111), (100), (110) and (210) electrodes in contact with a $NaClO_4$ 0.1 M, KCN 25 mM solution; scan rate 100 mV/s

crystal orientation. The anodic peaks have been interpreted as corresponding to: (A) CN^- adsorption on Au(hkl), (B) oxidative adsorption of CN^- on Au, giving rise to the formation of a surface species of the type $Au(I)–CN^-_{ads}$ and (C) Au oxidation giving rise to the formation of bulk Au $(CN)_2^-$. For details on mechanistic aspects of the voltammetric behaviour of the Au/CN^- system, see [11] and references therein quoted.

In our data, it is worth observing a tiny shoulder (*E*) on the cathodic-going scans in the high anodic range, which can be related to the Au mass-transport controlled reduction of $Au(I)–CN^-$ species to $Au°–CN^-$, which is well known to be the reduction intermediate at low overvoltages [26]. The exact location of the above-discussed features depends on the specific system. In the case of the single-crystal electrodes, these positions are determined by the kind of crystal face. Our results show a first anodic peak (A) located in the potential range −650 to −700 mV, a second positive peak (B) found between −100 and −500 mV and a third one (C) at the highest investigated anodic potentials. The cathodic peak (*D*) appears in the range −850 to −950 mV, again depending on the system.

The approximate peak positions which can be derived from the voltammograms of Fig. 2 are reported in Table 1. It is not our intention here to perform a quantitative and mechanistic analysis of the peak positions, but simply to rationalise our data in terms of the crystallographic nature of the electrode surface.

From the results reported in Table 1, the following conclusion can be drawn:

peak (A): higher cathodic potentials for the adsorption peak correspond to more open faces. This behaviour can be explained by the fact that CN^- absorption onto Au° is energetically favoured at more open faces;

peak (B): higher anodic potentials correspond to more compact faces. Oxidative adsorption thus seems easier at more open faces;

peak (D): higher cathodic potentials correspond to more open faces. This can be interpreted as an indication of the fact that desorption is easier from more compact faces. In is worth noticing that CN^- adsorbed onto poly-Au seems still more stable with respect to desorption [16], possibly owing to stabilisation at defect sites.

In summary, one can conclude that the adsorption of CN^- onto progressively more open faces seems to be increasingly irreversible (i.e. the distance between adsorption and desorption peaks increases).

In situ SFG and DFG spectroscopies

The potential-dependent electrodic behaviour of CN^- at Au (111), (100), (110) and (210) electrodes has been studied by in situ SFG and DFG spectroscopies. In all the spectra measured, a single resonance appears on the range 2,090–2,140 cm^{-1} due to CN^- stretching. Potential-dependent SFG and DFG spectra for the four crystal orientations investigated are reported in Figs. 3, 4, 5, 6, 7, 8, 9 and 10.

On the basis of [10, 27–29], these spectra have been analysed quantitatively with the following model:

$$I_{\mathrm{SFG/DFG}} \propto \left|\chi^{(2)}\right|^2 \text{with}$$
$$\chi^{(2)} = \chi^{(2)}_{\mathrm{ads}} + \chi^{(2)}_{\mathrm{met}} = \frac{A(V)}{\nu_{\mathrm{IR}} - \nu_0(V) \pm i\Gamma_{\mathrm{SFG/DFG}}} + a + i \cdot b \quad (1)$$

where:

(1) $\chi^{(2)}$ is the second-order surface susceptibility. It comprises two contributions to the SFG signal: $\chi^{(2)}_{\mathrm{ads}}$ is the resonant part arising from the adsorbates, whereas $\chi^{(2)}_{\mathrm{met}}$ is the part due to the metallic substrate;

(2) *A* is the resonator intensity, a function of potential *V* and coverage degree with CN^- θ. The potential dependence of *A* derives from the potential dependence of the quantities $\rho_a(E_F)$, α_V, α_e and *U* [29] where: $\rho_a(E_f)$ is the density of states at the Fermi level E_f of the adsorbate orbital involved in the dynamic coupling phenomenon; α_v and α_e are the vibrational and electronic parts of the molecular polarisability of the molecule undergoing adsorption; *U* is a term

Table 1 Approximate peak positions for Au(hkl) voltammograms, $NaClO_4$ 0.1 M, KCN 25 mM, atomic surface densities are reported for each crystal orientation

	(A) mV vs Ag/AgCl	(B) mV vs Ag/AgCl	(D) mV vs Ag/AgCl
Au(111) asd=2.3094 atoms/$Å^2$	−600	0	−725
Au(100) asd=2.0 atoms/$Å^2$	−620	−100	−750
Au(110) asd=1.4142 atoms/$Å^2$	−700	−125	−800
Au(210) asd=0.8165 atoms/$Å^2$	−700	−200	−800

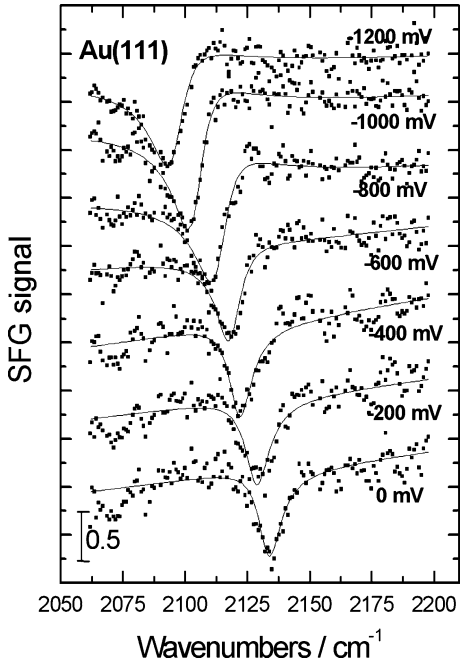

Fig. 3 Potential-dependent SFG spectra (*squares*) and results of the fit with the $|\chi^{(2)}|^2$ model (*continuous line*) for the Au(111) electrode in contact with a $NaClO_4$ 0.1 M, KCN 25 mM solution

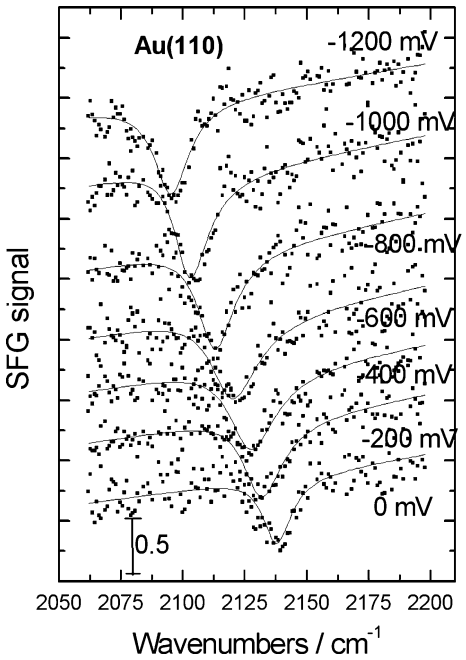

Fig. 5 Potential-dependent SFG spectra (*squares*) and results of the fit with the $|\chi^{(2)}|^2$ model (*continuous line*) for the Au(110) electrode in contact with a $NaClO_4$ 0.1 M, KCN 25 mM solution

accounting for local field effects on the induced dipole of the adsorbate;

(3) ν_{IR} is the scanned IR frequency;

(4) $\nu_o(V) \cong \nu_{free} + a_2 + b_2 V + c_2 V^2$ is the potential-dependent resonant frequency, ν_{free} is the singleton frequency, a_2 and b_2 account for the potential dependence of $\rho_a(E_F)$, U, α_V, α_e and θ [11];

(5) $\Gamma_{SFG/DFG}$ is the resonator broadening;

(6) a and b are the model constants, relating to the free-electron (a) and bound-electron "b" contributions to

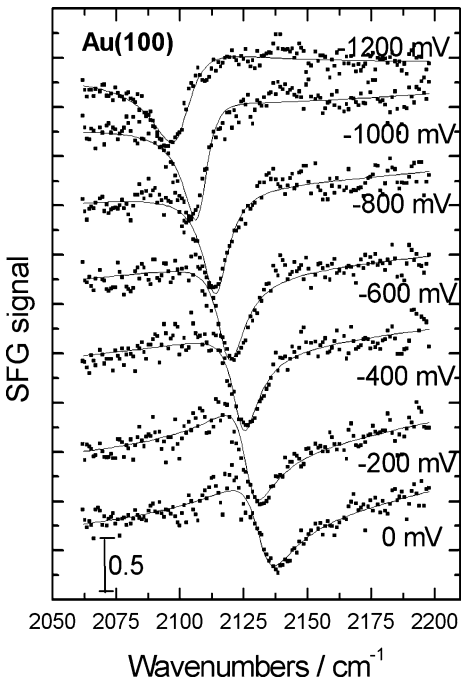

Fig. 4 Potential-dependent SFG spectra (*squares*) and results of the fit with the $|\chi^{(2)}|^2$ model (*continuous line*) for the Au(100) electrode in contact with a $NaClO_4$ 0.1 M, KCN 25 mM solution

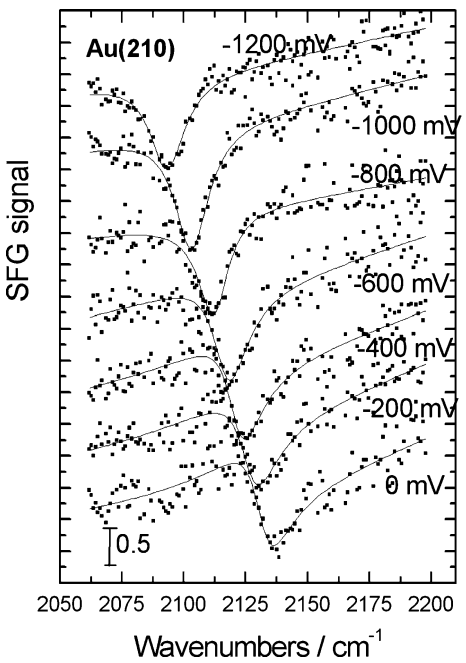

Fig. 6 Potential-dependent SFG spectra (*squares*) and results of the fit with the $|\chi^{(2)}|^2$ model (*continuous line*) for the Au(210) electrode in contact with a $NaClO_4$ 0.1 M, KCN 25 mM solution

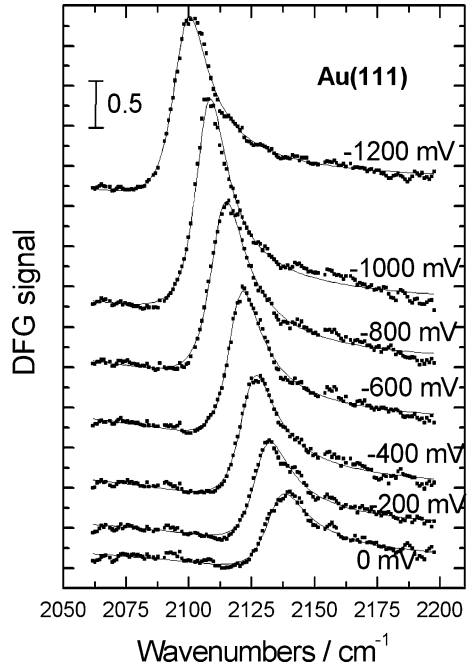

Fig. 7 Potential-dependent DFG spectra (*squares*) and results of the fit with the $|\chi^{(2)}|^2$ model (*continuous line*) for the Au(111) electrode in contact with a $NaClO_4$ 0.1 M, KCN 25 mM solution

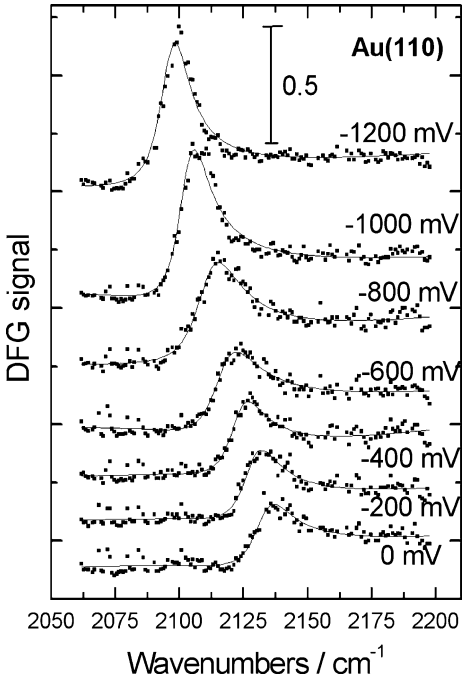

Fig. 9 Potential-dependent DFG spectra (*squares*) and results of the fit with the $|\chi^{(2)}|^2$ model (*continuous line*) for the Au(110) electrode in contact with a $NaClO_4$ 0.1 M, KCN 25 mM solution

non-resonant term; "*a*" is essentially related to the surface charge density, while "*b*" is proportional to the population of bound electronic states with energy h ($\nu_{VIS} \pm \nu_{IR}$; for details, see [10, 29]).

Interference effects can be quantified in terms of the contrast parameter c proposed in [27]:

$$c = 2\left|\chi_r^{(2)}\right|\left|\chi_{nr}^{(2)}\right| \Big/ \left[\left|\chi_r^{(2)}\right|^2 + \left|\chi_{nr}^{(2)}\right|^2\right]. \quad (2)$$

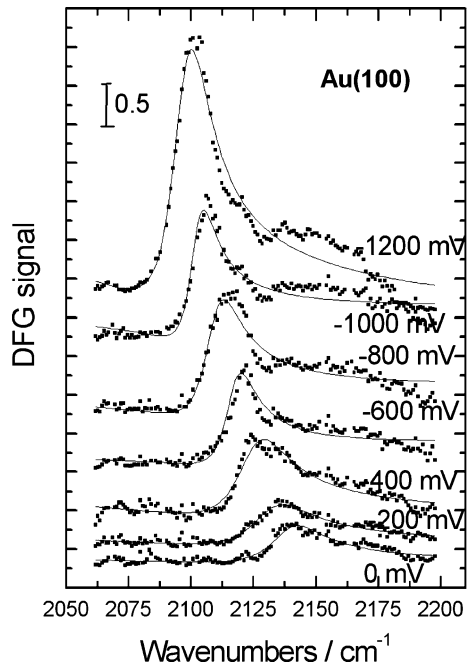

Fig. 8 Potential-dependent DFG spectra (*squares*) and results of the fit with the $|\chi^{(2)}|^2$ model (*continuous line*) for the Au(100) electrode in contact with a $NaClO_4$ 0.1 M, KCN 25 mM solution

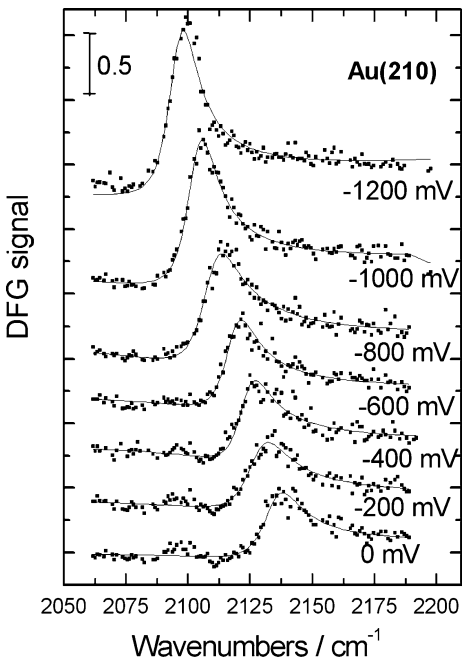

Fig. 10 Potential-dependent DFG spectra (*squares*) and results of the fit with the $|\chi^{(2)}|^2$ model (*continuous line*) for the Au(210) electrode in contact with a $NaClO_4$ 0.1 M, KCN 25 mM solution

The fit parameters were identified as a function of potential with a minimisation procedure based on the Levemberg–Marquart algorithm. Of course, it is not straightforward to work out functional dependences from NLLS, owing to the presence of local minima (see, e.g. [30]); to cope with this problem, we resorted to using a continuation method based on using as guess values the parameter values identified for a physically close condition.

In the currently implemented version of the SFG/DFG spectroscopies, the absolute value of $I_{SFG/DFG}$ depends on the settings of the laser and of the optics. These quantities are fixed during the alignment and optimisation procedure for the system corresponding typically to a given set of SFG and DFG experiments. From this fact, it follows that comparison among crystal orientations and SFG/DFG experiments must be done with respect to quantities that are independent of the particular experimental mounting. It can be straightforwardly verified that these quantities are: ν_o, Γ, ϕ=atan(b/a) and c. Reliable information for comparison can also be derived by normalising A with respect to the maximum of a given set of potential-dependent experiments. One note of caution is worth making on the procedure used to estimate "b". Our spectra exhibit a linear trend of the non-resonant background, which, in principle, might derive from the wavelength-dependence of "b", but is essentially due to subtle setup transmission-function properties that are not yet fully understood. An efficient and reliable method to cope with this problem is to allow for a linear wavelength dependence for "b" in the NLLS model and, after convergence has been achieved, to set "b" equal to the values found at 2,000 cm^{-1}. The confidence intervals for this estimate of "b" were derived from those of the two-parameter linear model with a statistical transformation defined along the lines of [31].

The potential dependence of the SFG and DFG spectra can be interpreted in terms of the discussions proposed in [10–12]: the chief results can be summarised as follows:

(1) the oxidative desorption potential of CN^- is independent from the crystal face;

(2) the adsorption potentials are: −1,300, −1,000 and −800 mV vs SCE for Au(110), (100) and (111), respectively, denoting that the adsorption energy tends to increase with face openness and correlates positively with the pzc;

(3) the desorption rate of CN^- correlates positively with the slope of resonator strength vs potential curves; higher slopes were measured for Au(111) than for (100) and (110);

(4) the Stark shift is parabolic and independent on the crystal orientations studied, denoting that the bonding site is the same, regardless of the atomic packing of the surface considered;

(5) the resonance broadening is independent from crystal orientation and potential, suggesting that a homogeneous broadening mechanism dominates.

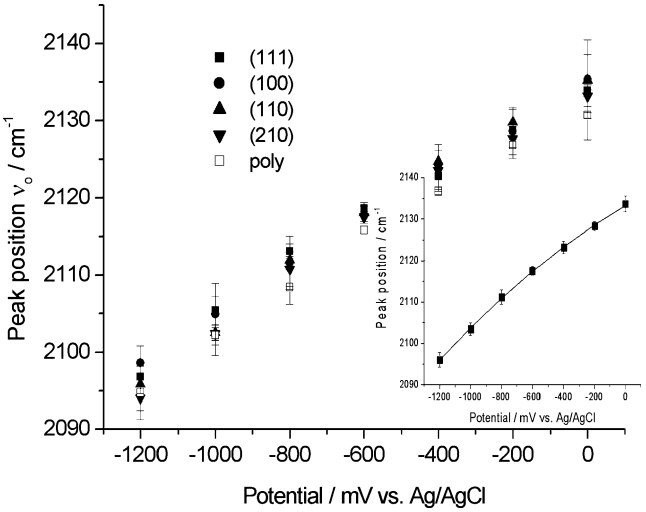

Fig. 11 Potential-dependent peak positions ν_o estimated with the Eq. 1 from SFG and DFG spectra for Au(111), (100), (110) and (210) single-crystal and polycrystalline Au electrodes in contact with a $NaClO_4$ 0.1 M, KCN 25 mM solution. *Inset* Averages over all the investigated crystal orientations (*squares*) ±1 standard deviation and result of a parabolic fit (*continuous line*)

The present paper confirms this view, extends the availability of experimental data to the (210) orientation and to the combination of SFG and DFG and proposes some conclusions regarding the non-resonant part of the second-order susceptibility.

Peak position of the vibrational resonance ν_o

Our results concerning the potential dependence of the peak position of the vibrational resonance ν_o are summarised in Fig. 11. Error bars are the results of the evaluation of 95% confidence intervals and data pooling according to the procedure illustrated below. Analysis of our raw data indicates that no quantitative differences are found between SFG and DFG data. This result is actually expected from the theory of electrochemical SFG [10]; therefore, regarding ν_o, use of SFG and DFG simply improves the statistical reliability of the data. The corresponding values for each electrode considered are therefore pooled in Fig. 11. Inspection of Fig. 11 shows that no measurable differences in ν_o emerge among the different crystal orientations studied. A simple parabolic fit can thus be carried out pooling all the data using the computed errors as weights for the linear regression; the results are reported in the inset of Fig. 11. The following parameter values were obtained $\nu_{free}+a_2$=2,133.2±0.3 cm^{-1}, b_2=

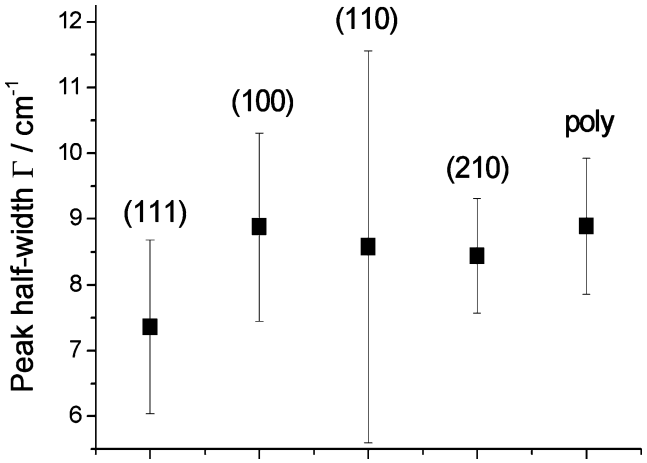

Fig. 12 Peak half-width Γ estimated with the Eq. 1 from potential-dependent SFG and DFG spectra for Au(111), (100), (110) and (210) single-crystal and polycrystalline Au electrodes in contact with a $NaClO_4$ 0.1 M, KCN 25 mM solution

21.70±1.15 V−1 cm^{-1}, c_2=−7.78±0.92 V^{-2} cm^{-1}, ρ^2= 1.000. These parameter values are consistent with those derived from SFG spectra from (111) and (210) crystals in [11]. Our results confirm the view first expressed in [10], that CN^- adsorbs on Au on a single site regardless of the crystal orientation. This conclusion extends also to polycrystalline Au, showing that the presence of grain boundaries plays no role as far as the kind of adsorption site is concerned.

Peak half-width of the vibrational resonance Γ

No statistically significant differences are found between SFG and DFG, as expected for single vibrationally resonant

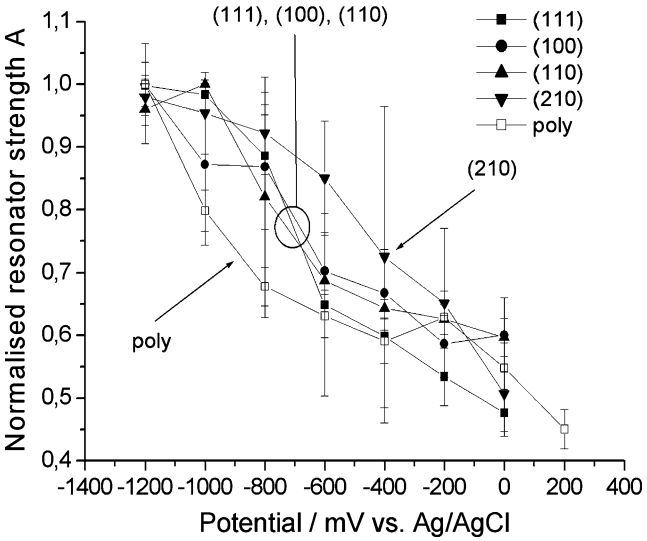

Fig. 13 Potential-dependent normalised resonator strengths A_N estimated with the Eq. 1 from SFG and DFG spectra for Au(111), (100), (110) and (210) single-crystal and polycrystalline Au electrodes in contact with a $NaClO_4$ 0.1 M, KCN 25 mM solution

spectroscopy. We did not find statistically meaningful variations of Γ as a function of potential either. This result is correlated with the single adsorption site scenario envisaged in "Peak position of the vibrational resonance ν_o". For purposes of data presentation, we have pooled all the potential-dependent SFG and DFG data obtained for each type of electrode to estimate a single expected value and corresponding error. These quantities are represented in Fig. 12, which suggests that the surface atomic packing and the presence of grain boundaries have no apparent impact on the resonance broadening mechanism.

Normalised resonator strength A_N

The potential-dependent values of A_N are reported for the electrodes studied in Fig. 13. No statistically significant differences were found between the parameters evaluated by SFG and DFG; data derived from the tow spectroscopies are therefore pooled in Fig. 13. The comment made in "Peak half-width of the vibrational resonance Γ" about visible resonance hold also in this case. The normalised resonator strength tends to decrease with increasing potential, owing to anodic desorption of CN^-, coherently with our CV results, and the data reported in [10, 11]. From the slope of these curves, conclusions regarding desorption rates were derived in [10]. In this case, we analysed this set of data in terms of Frumkin isotherm [32]. Under the assumption that the adsorption energy E_{ADS} is the same for all orientations (see the single-site scheme discussed in "Peak position of the vibrational resonance ν_o") and the PZC in the absence of CN^- adsorption are known, the lateral interaction energy E_{LI} can be estimated. By straightforward algebra, it can be shown that at the flex of the $\theta-V$ isotherm:

$$\frac{E_{LI}}{RT} = 2\left[\frac{\Phi F}{RT}\right]^{E_{ADS}\cdot C} \tag{3}$$

where C stands for the bulk concentration of CN^-, $\Phi = V_o - E_{PZC}$, and V_o is the potential at which the flex of the experimental A_N vs potential curves. E_{PZC} values can be obtained from [33] for (111), (100) and (110) and from [18] for (210) and from [34] for polycrystalline Au. As literature values for E_{ADS} are not available, to the best of authors' knowledge, we resorted to estimating the sequence of Φ values and which correlates positively with that of E_{LI} ones. We found the following sequence of Φ: (111) −972± 105 mV, (100) −975±165 mV, (110) −901±104 mV, (210) −510±185 mV, poly-Au −1243±59 mV.

A stability hierarchy seems to emerge from our data: poly-Au<(111)≅(110)≅(110)<(210). The (210) orientation, with the lowest atomic packing among the single-crystal

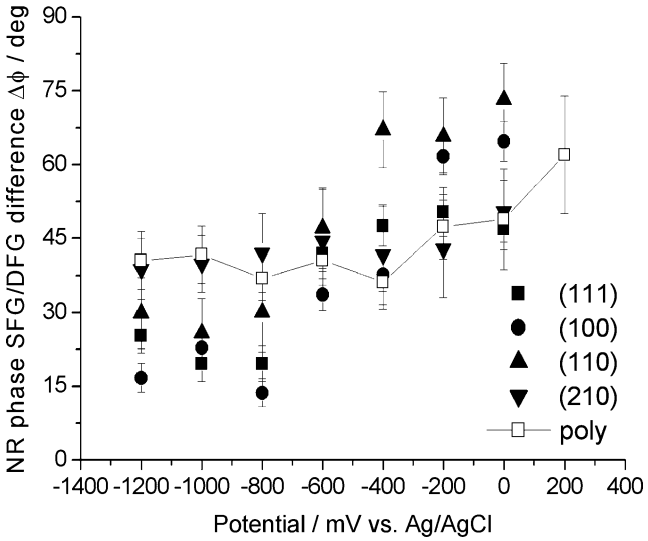

Fig. 14 Potential-dependent differences $\Delta\phi$ between the phases of the non-resonant contribution obtained by SFG and DFG for Au(111), (100), (110) and (210) single-crystal and polycrystalline Au electrodes in contact with a $NaClO_4$ 0.1 M, KCN 25 mM solution

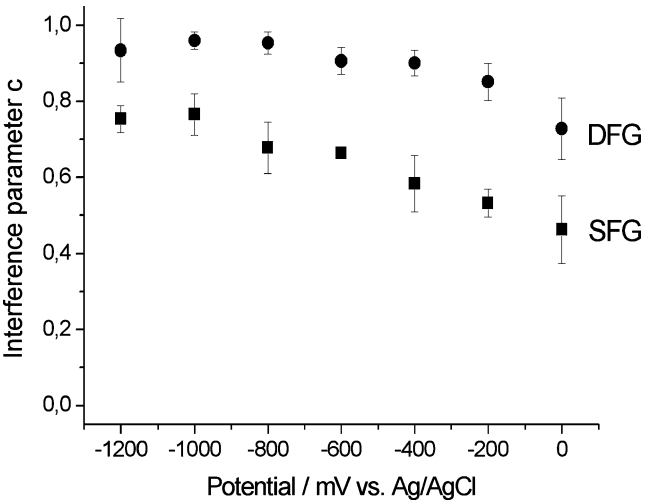

Fig. 15 Potential-dependent contrast parameter c estimated from SFG and DFG measurements with Au(111), (100), (110) and (210) single-crystal and polycrystalline Au electrodes in contact with a $NaClO_4$ 0.1 M, KCN 25 mM solution. Data points obtained as averages over all the investigated crystal orientations

surfaces considered, exhibits the smallest lateral repulsion, while the polycrystalline electrode shows the highest one for some subtle reasons, possibly related to the presence of grain boundaries.

Difference between the phases of the non-resonant term of SFG and DFG spectra $\Delta\phi_{NR}$

As commented above, ϕ is a descriptor of the non-resonant contribution to the second-order susceptibility that is independent on the setup details (see "In situ SFG and DFG spectroscopies"). Its definition for SFG and DFG is discussed in detail in [27] pp 58, 70 and [10]. For the present purpose, we shall concentrate on the following aspects, enabling us to derive information regarding the electronic structure of the probed interface. If far from the interband transition of the substrate metal, $\phi_{SFG} \cong \phi_{DFG}$, otherwise $\Delta\phi \neq 0$. From the experimental values of ϕ reported on [27] (pp 50s, 55s and 59s), we computed the following representative $\Delta\phi$ values: Au +43°, Ag −28° and Pt 0°.

In Fig. 14, we report our potential-dependent results for the five electrodes studied. Similar growing trends are found for all the electrodes; lower slopes correspond to the more open (210) face and to the defective poly-Au one. The potential dependence of $\Delta\phi_{NR}$ correlates to that of the surface DOS D_S, in this way: $\Delta\phi_{NR}(V_A) > \Delta\phi_{NR}(V_B)$ implies $\partial D_S(V_A)/\partial\omega > \partial D_S(V_B)/\partial\omega$. An insightful understanding of this point requires electronic structure modelling of the interface beyond the possibilities of this investigation, which nevertheless points means to stress the fact that the effects of adsorption, crystal orientation and potential on the electronic structure of the electrochemical interface can be reliably derived from a suitable combination of SFG and DFG spectroscopies.

Contrast parameter c

The contrast parameter has been evaluated at resonance ν_o. Very minor differences are found among the different electrodes studies, while a clear potential dependence emerges as well as differences between SFG and DFG. Pooled data for the five electrodes are reported in Fig. 15. As in the absence of visible resonances $|\chi_R^{SFG}(\nu_o)| = |\chi_R^{DFG}(\nu_o)| = |\chi_R(\nu_o)|$, while in general $|\chi_{NR}^{SFG}| \neq |\chi_{NR}^{DFG}|$, it follows that our data imply: $|\chi_{NR}^{DFG}| \cong |\chi_R(\nu_o)| \neq |\chi_{NR}^{SFG}|$, corresponding to the fact that $c^{DFG} \cong 1$, while $c^{SFG} < 1$. Of course, full understanding of this quantity requires the knowledge of the interactions between the electronic structure of the metallic electrode as affected by the adsorbate and the applied potential and the surface coverage with the adsorbate. This is beyond the scope of the present paper, but we maintain that access to statistically significant estimates of such observables is a precious tool for the understanding of the electrochemical interface.

Conclusions

Our in situ DFG and SFG data on the electrochemical adsorption of CN^- on Au(111), (100), (110) and (210) electrodes confirm previous results obtained by DFG on Au (111), (100) and (110) and by both SFG and DFG on Au (100) and extend the study of this system to Au(210)

and complete the comparison between SFG and DFG spectroscopies.

The experimental spectra were analysed quantitatively to extract parameters that can give information on the vibrational and electronic structure of the interface.

The analysis of the vibrational resonant frequency and of the resonance width indicate that a single adsorption site for CN^- is found on Au electrodes of different crystal orientations. The potential dependence of the resonator intensity yields information on the lateral interaction energy of adsorbed CN^-. Our results indicate that the lateral interaction energy correlates negatively with surface atomic density.

By comparing the phase of the non-resonant part of the spectra measured by SFG and DFG, one can obtain information on the slope of the surface electronic DOS in the vicinity of the energy of the visible beam under the current electrochemical conditions. The information derived from the non-resonant component of the second-order susceptibility, as well as from the contrast parameter, provide unambiguous evidence of the fact that CN^- adsorption onto Au single crystals gives rise to a rich potential-dependent scenario of modifications of the electronic structure of the interface.

Acknowledgements Highly qualified and continuous technical assistance is gratefully acknowledged to the SFG collaborators and CLIO staff, Bâtiment 209D, Centre Universitaire Paris Sud, 91405 Orsay, France.

References

1. Baltruschat H, Heitbaum J (1983) J Electroanal Chem 157:319
2. Corrigan DS, Gao P, Leung LH, Weaver MJ (1986) Langmuir 2:744
3. Gao P, Weaver MJ (1989) J Phys Chem 93:6205
4. Kunimatsu K, Seki H, Golden WG (1984) Chem Phys Lett 108:195
5. Kuminatsu K, Seki H, Golden WG, Gordon JG, Philpott MR (1985) Surf Sci 158:596
6. Pettinger B, Picardi G, Schuster R, Ertl G (2003) J Electroanal Chem 554–555:293
7. Sawaguchi T, Yamada T, Okinaka Y, Itaya K (1995) J Phys Chem 99:14149
8. Tadjeddine M, Flament JP (1999) Chem Phys 240:39
9. Beltramo GL, Shubina TE, Mitchell SJ, Koper MTM (2004) J Electroanal Chem 563:111
10. Tadjeddine A, Le Rille A (1999) In: Wieckowski A (Ed) Interfacial electrochemistry: theory, experiment and applications. Dekker, New York, p 317
11. Bozzini B, Mele C, Fanigliulo A, Busson B, Vidal F, Tadjeddine A (2004) J Electroanal Chem 574:85
12. Le Rille A, Tadjeddine A, (1999) J Electroanal Chem 467:238
13. Matranga C, Guyot-Sionnest P (2000) J Chem Phys 112:7615
14. Matranga C, Wehrenberg B, Guyot-Sionnest P (2002) J Phys Chem B 106:8172
15. Hamelin A, Katayama A (1981) J Electroanal Chem 117:221
16. Bozzini B, Busson B, De Gaudenzi GP, Mele C, Tadjeddine A (2007) J Alloys Compd 427:341
17. Mani AA, Dreesen L, Hollander Ph, Humbert C, Caudano Y, Thiry PA, Peremans A (2001) Appl Phys Lett 79:1945
18. Motheo AJ, Santos Jr JR, Sadkowski A, Hamelin A (1995) J Electroanal Chem 397:331
19. Hamelin A (1996) J Electroanal Chem 407:1
20. Hamelin A, Martins AM (1996) J Electroanal Chem 407:13
21. Dakkouri AS, Kolb DM (1999) In: WieckowskiA (Ed) Interfacial electrochemistry. Dekker, New York, p 151
22. Hamelin A (1995) J Electroanal Chem 386:1
23. Hamelin A, Stoicoviciu L, Edens GJ, Gao X, Weaver MJ (1994) J Electroanal Chem 365:47
24. Bozzini B, Cavallotti PL (2001) J Electrochem Soc 148:C231
25. Fanigliulo A, Bozzini B (2003) Corrosion Eng Sci Technol 38:228
26. Bozzini B, Giovannelli G, Natali S, Fanigliulo A, Cavallotti PL (2002) J Mater Sci 37:3903
27. Le Rille A (1997) Thèse de doctorat, Université de Paris-sud
28. Pluchery O (2000) Thèse de doctorat, Université Paris XI
29. Vidal F (2003) Thèse de doctorat, Université Paris XI
30. Sgura I, Bozzini B (2005) Numerical issues related to the modelling of electrochemical impedance data by non-linear least-squares. Int J Non-Linear Mech 40(4):557–570
31. Bozzini B, Boniardi M, Fanigliulo A, Bogani F (2001) Mat Res Bull 36:1889
32. Gileadi E (1993) Electrode kinetics. VCH Publishers Inc, New York, p 267
33. Trasatti S (1995) Surf Sci 335:1
34. Dahms H, Green M (1963) J Electrochem Soc 110:1075